FACULTY OF PSYCHOLOGY AND EDUCATIONAL SCIENCES

A REPRODUCIBLE PIPELINE FOR ERP GROUP STUDIES USING THE MNE SOFTWARE

Case studies in the analysis of experimental data

Pieter De Clercq

Supervisor: Prof. Dr. Daniele Marinazzo

Academic year: 2019-2020

GHENT UNIVERSITY

Abstract

In the present study, we provide a reproducible pipeline for analyzing EEG (ERP) group data in python using the MNE software. We provide recommendations and common good practices in preprocessing steps, grand averaging, statistical analyses and source localization techniques. Data files were acquired from an EEG group study at Ghent University that embarks on the influence of emotion on spatial vision. Hence data was only acquired from 3 good pilots yet, we limit current analyses to the divergent electrical responses evoked by Low Spatial Frequent (LSF) and High Spatial Frequent (HSF) grating stimuli in order to obtain considerably more trials.

Introduction

A short discussion of the study and its main outstanding research questions we base our analyses on in this pipeline, is provided in Appendix A. We strongly recommend to go through this Appendix. By doing so, the reader can fully understand the main goal of the analyses and the different conditions/epochs we created in this pipeline. Moreover, the Appendix provides information on the EEG data recording in Biosemi (BioSemi B. V., Amsterdam, the Netherlands), external electrodes that were placed, sampling rate and online referencing of the data.

We will now discuss our pipeline for ERP group studies in Python (version 3.7.) using the MNE software (Gramfort, Strohmeier, Haueisen, Hämäläinen, & Kowalski, 2013).

(Pre-)Processing steps

1. Data File Reorganization

First, we read our raw Biosemi data file into MNE. Information on the recorded dataset can be obtained via raw.info() line of code. MNE further provides convenient code to rename channels and reset channel types. The latter step is quite useful; users can then flexibly pick EEG channels for re-referencing purposes or pick EOG channels for ocular corrections for example. Finally, it is important to set the EEG-cap montage so topographical maps could be made or source localization analyses could be run.

2. Raw Data Cleaning

2.1. Interpolating Bad Channels

After the file is reorganized to the user's preferences, researchers can then identify and repair bad channels. One can look for bad channels online (i.e. during the scan session), or after data collecting by

plotting the raw data. Perhaps the most convenient way to look for bad channels and other spectral artifacts however, is by plotting the Power Spectral Density (PSD) of each channel separately. MNE computes the PSD of raw data using the standard Welch's method (Welch, 1967; Percival and Walden, 1993), whereby the signal for each channel is analyzed over consecutive time segments. Each segment is windowed and then the power of the discrete Fourier transform (DFT) coefficients is computed and averaged over all segments. In our pilots, we identified no bad channels or spectral artifacts. An example for a single subject is provided in Appendix B. Highly increased power at the lowest (<1Hz) or highest (>50Hz) frequencies for single electrodes for example, is something to be suspicious about (Jas et al., 2018). Bad EEG channels should then be repaired by spherical spline interpolation (Perrin, Penier, Bertrand, & Echallier, 1989) rather than removing bad channels for the purpose of group averaging.

2.2. Re-referencing

Although the channels are online referenced in Biosemi, it is important to re-reference the data post-hoc, because EEG voltages recorded at each electrode are relative to voltages recorded at other electrodes. This is typically done by referencing the EEG electrodes to the electrodes placed on the mastoids or by referencing to the average of all electrodes. Since the former method is believed to contain some neural signals from temporal lobes nearby the ear and thereby a bias in the reference could be created, it is strongly recommended to reference the data to the average of all electrodes (Choi & Hwang, 2019).

2.3. Band-pass filtering the Data

Next, we band-pass filtered the data. We focused on event-related brain signals below 40Hz, so we applied a low-pass filter. In order to remove slow artifacts, we high-pass filtered the data at 0.01Hz. A recent study demonstrated that high-pass filters at 0.01Hz or 0.1 Hz are optimal, while higher filters could significantly decrease power and increase the likelihood of creating artifactual effects (Tanner, Morgan-Short & Luck, 2016). Another useful filter to apply is the notch-filter at 50Hz, which cancels out electrical noise. Since our low-pass filter was sufficiently low, we did not need to apply this filter.

3. Epoching and Further Data Cleaning

Subsequently, we extracted data segments from the continuous signal around our events of interest. They are stored as single trials (i.e. Epochs) in MNE. The Epochs object can store data from multiple events and the researcher can conveniently call a subset of events with “epochs[event_id]” line of code. Moreover, MNE software provides the opportunity to hierarchically store the conditions in a dictionary. This is our dictionary containing all relevant conditions for the current study with its event markers:

```
events_id = {'LSF/C/REF': 20, 'LSF/C/TEST': 30, 'LSF/BT/REF': 40, 'LSF/BT/TEST': 50,
'LSF/PST/REF': 60, 'LSF/PST/TEST': 70, 'HSF/C/REF': 25, 'HSF/C/TEST': 35,
'HSF/BT/REF': 45, 'HSF/BT/TEST': 55, 'HSF/PST/REF': 65, 'HSF/PST/TEST': 75}
```

At the highest level of hierarchy are LSF and HSF. These are the main conditions our analyses focus on in this pipeline. We can conveniently access these conditions by using epochs['LSF'] or epochs[‘HSF’] and MNE internally pools all the sub-conditions together.

3.1. Ocular Correction

In the present study, we used Independent Component Analysis (ICA) to decompose the signal into maximally independent components. In the context of EEG, ICA is commonly used to correct for or remove systematic physiological artifacts that affect multiple sensors. These artifacts have skewed and peaky distributions, hence easily captured by ICA. We applied ICA here to identify and remove eye blinks. This can be done manually as we show in Appendix C for a single subject. Based on the topographical maps and the ICA sources, we identified component 006 as the component that captures eye-blinks. We then excluded this component manually and plotted the raw data again (Appendix C, 3. and 4.). It is clear that our data is now cleared from ocular artifacts.

This step can be done automatically as well. This is quite useful in order to run our preprocessing steps parallel across all subjects. In MNE, ICA identifies the component based on the EOG events the user needs to create a priori. Identifying and removing bad EOG epochs can be achieved by means of convenient code: eog_inds=ica.find_bads_eog(eog_epochs), and ica.exclude(eog_inds). Finally, it is important to include all channels (including EEG, mastoids, EOG and eventual other external electrodes) in ICA and first to *fit* ICA on the raw data (ica.fit(raw)). Later on, ICA is *applied* on the epochs (ica.apply(epochs)).

3.2. Baseline correction

It is common practice to use baseline correction so that any constant offsets in the baseline are removed. In this way, researchers can clearly look at the neural response evoked by the stimuli presentation. In MNE, baseline correction can be done when the user creates the epochs. We have set the baseline from the start of the epoch (-200ms) to stimulus onset (0ms).

3.3. Artifact rejection

In MNE, clearing data from bad trials can be achieved by removing trials whose peak-to-peak amplitude exceeds a certain rejection threshold (indicating too much artifacts). This threshold can be set manually (for example at ±80 μV), or learned from the dataset itself with the ‘autoreject’ algorithm (Jas et

al., 2017). Autoreject is an unsupervised algorithm which minimizes the cross-validation error, measured by the Frobenius norm between the average signal of the training set and the median signal of the validation set. It removes trials containing transient jumps in isolated EEG channels, or for example eyeblink artifacts affecting groups of channels in the frontal area. We chose to reject trials based on this algorithm. Percentage of trial rejection was never higher than 20% and more or less equal across conditions. This is no problem considering our large number of LSF and HSF trials (n=300).

4. Evoked Data

Then, we averaged all epochs per condition, per participant, per channel. This is stored in the 'Evoked' object in MNE. This object represents all ERP's, for all channels, participants and conditions separately.

Sensor Space Analysis

1. Grand Averaging

A classical step in EEG group studies is known as "grand averaging" (Delorme, Miyakoshi, Jung, & Makeig, 2015). This step consists of averaging ERPs across all subjects in the study. As not all subjects have generally the same good channels, this step is commonly preceded by an interpolation step to make sure data are available for all channels and for all subjects. Appendix D visualizes our two clusters of interest (Cluster 1: Oz, O1 and O2 for the N80 and P1 component; Cluster 2: PO7 and PO8, for the N1 component). The clusters were picked based on relevant literature, which is summarized in Appendix A. All datapoints from electrodes in one cluster are commonly averaged. In our grand average plots in Appendix D, we can already observe some remarkable differences between the LSF and HSF condition: In line with previous research, HSF stimuli evoke a negative-going peak around 80ms which seems absent in LSF stimuli, together with longer latencies for the P1 and N1, and a stronger amplitude peak for the N1 component (although relying on only 3 pilots for now…).

2. Contrasting conditions

In the current pipeline, we base analyses on the difference between the LSF and HSF condition. Before the group level tests, we need to compute the contrast between LSF and HSF for each subject. We obtain this contrast by subtracting the evoked responses of the LSF condition to the HSF condition. The conditions were weighted equally, so it takes the number of trials per condition (most likely not perfectly equal) into account to compute the evoked response.

The contrast between LSF and HSF is visualized in Appendix E. One can clearly observe the importance of carefully pre-specifying the electrode-clusters of interest: The difference around the P1 is

largest in the occipital cluster, while the difference around the N1 is largest around the parieto-occipital cluster.

Statistical Analyses

To investigate statistical significant differences between LSF and HSF, we used cluster-based permutation F-tests. This technique is commonly used in EEG studies. It avoids the multiple comparison problem: Instead of performing a statistical test for each time point individually, clusters of time-points are defined by an arbitrary cut-off point ($p<0.05$). Then, a single permutation F-test is performed on a single cluster. In MNE, the researcher can define the threshold manually, or automatically by MNE; if threshold is set to 'None', an F-threshold will be chosen automatically that corresponds to a p value<0.05 for the given number of observations.

In the present study, we can visually identify 2 clear peaks in the contrast condition (Appendix E): One at 72ms, the other at 160ms. However, no significant F-values were returned (perhaps due to the small number of observations for now). Further data collection is required to establish the differences in both conditions.

Source Localization

Although the temporal resolution of EEG is superior compared to other popular neuro-imaging methods (fMRI for example), the spatial resolution is inferior. Source estimation based on the measured signal is challenging, and often contaminated. The source localization problem is divided in two components: the forward and inverse problem. The former problem is solved by predicting the effects of results for a set of known parameters. In the latter problem however, we typically start from the observed data and infer what parameters caused the data. The number of parameters are assumed to be greater than the number of electrodes, therefore the problem is 'ill-formed' (Grech et al., 2008). Numerous mathematical methods and measurement techniques have been proposed to tackle this inverse problem (Khemakhem, Zouch, Hamida, & Taleb-Ahmed, 2009).

In this pipeline, we provide code to implement the forward solution, the covariance matrix[1] and the inverse solution in the contrast condition. A template MRI-brain was used to plot the source estimations. We further used the standardized low-resolution brain electromagnetic tomography (sLORETA, Pascal-Marqui, 2002) method to compute the inverse solution. Appendix F 1. depicts the time-series activation for our sources, F 2. and F 3. the 2-D source estimations for our 2 peaks in activation. The blue dot represents the point of maximum activation. As expected, the maximum activation spot moved slightly lateral in our second

[1] The covariance matrix is needed to compute the inverse solution. For an overview, see Grech et al., 2008.

peak (160ms) compared to the first peak (72ms, central occipital). We have also provided code to plot the orientations of the sources/dipoles, and they are visualized in F 4. and 5. . Finally, we ran another statistical cluster test across space and time (spatio-temporal clustering). Because the cluster test in time-series was not significant, the spatio-temporal was not significant as well. Nonetheless, code for future researchers is provided as well.

Discussion

The current project aimed to provide a practicable and reproducible pipeline for the analysis of ERP-group data in MNE, Python. We mainly focused on how to properly implement pre-processing steps and to perform Grand Averaging for group purposes. Previous research demonstrated that lack of attention to the very early stages of an EEG pipeline can reduce the signal-to-noise ratio (Bigdely-Shamlo, Mullen, Kothe, Su, & Robbins, 2015). In the present study, we provided common good practices in preprocessing steps and hands-on code in MNE. Moreover, we provided code to perform statistical analyses using cluster-based permutation tests and to perform source localization using the sLORETA method (Pascal-Marqui, 2002). Finally, we recommend researchers interested in ERP group studies to familiarize themselves with issues concerning component overlap and component quantification. Moreover, when statistically testing the peak amplitude of the ERP-components, researchers could run peak-to-peak analyses as well (Mushtaq, Bland, & Schaefer, 2011). See the books by Luck and Handy (Handy, 2004; Luck, 2005) for more information of these issues and techniques.

References

Bigdely-Shamlo, N., Mullen, T., Kothe, C., Su, K.M. & Robbins, K.A. (2015). The PREP pipeline: standardized preprocessing for large-scale EEG analysis. *Front NeuroInform., 9,* 16.

Choi, S.I., & Hwang, H.J. (2019). Corrigendum: Effects of different re-referencing methods on spontaneously generated ear-EEG. *Front. Neurosci., 13,* 908.

Delorme, A., Miyakoshi, M., Jung, T.P., & Makeig, S. (2015). Grand average ERP-image plotting and statistics: A method for comparing variability in event-related single-trial EEG activities across subjects and conditions. *J. NeuroSci. Methods, 30, 250,* 3-6.

Gramfort, A., Strohmeier, D., Haueisen, J., Hämäläinen, M. S., and Kowalski, M. (2013b). Time-frequency mixed-norm estimates: Sparse M/EEG imaging with non-stationary source activations. *Neuroimage* 70, 410–422.

Grech, R., Cassar, T., et al. (2008). Review on solving the inverse problem in EEG source analysis. *J. Neuroeng. Rehabil., 5,* 25.

Handy, T.C. (2004). Event-related potentials. *A Bradford book.*

Jas, M., Engemann, D.A., Bekhti, Y., et al. (2017). Autoreject: Automatic artifact rejection for MEG and EEG data. *NeuroI, 1, 159,* 417-429.

Jas, M., Larson, E., Engemann, D.A., et al. (2018). A reproducible MEG/EEG group study with the MNE software: recommendations, quality assessments and good practices. *Front. Neursci., 12,* 530.

Khemakhem R., Zouch W., Hamida A.B., Taleb-Ahmed A., & Feki, I. (2009) EEG Source Localization Using the Inverse Problem Methods. *IJCSNS, 9,* 408.

Luck, S. J. (2005). An introduction to the event related potential technique. (M. S. Gazzaniga, Ed.). *Cambridge/London: MIT Press.*

Mushtaq, F., Bland, A. R., & Schaefer, A. (2011). Uncertainty and cognitive control. *Frontiers in Psychology, 2,* 249.

Pascual-Marqui, R. D. (2002). Standardized low-resolution brain electromagnetic tomography (sLORETA): tech-nical details. *Methods and Findings in Experimental and Clinical Pharmacology, 24,* 5–12.

Percival, D.B., & Walden, A.T. (1993). Spectral Analysis for Physical Applications. *Cambridge University Press.*

Perrin, F., Penier, J., Bertrand, O., & Echallier, J.F. (1989). Spectral splines for scalp potential and current density mapping. *Electrenc. And Clinical Neurphysiol., 72(2),* 184-187.

Tanner, D., Morgan-Short, K., & Luck, S.J. (2016). How inappropriate high-pass filters can produce artifactual effects and incorrect conclusions in ERP studies of language and cognition. *Psychophysiology, 52(8),* 997-1009.

Welch, P. (1967). The use of fast Fourier transform for the estimation of power spectra: A method based on time averaging over short, modified periodograms. *IEEE Transactions on Audio and Electroacoustics, 15 (2),* 70-73.

Appendix A: Study Information

1. Literature Overview

The study at Ghent University explored the impact of fear on spatial vision. Spatial vision refers to the ability to discriminate spatially defined features. Two primary measures of spatial vision are traditionally proposed; acuity and contrast sensitivity. The latter measure is what the study focused on.

Contrast sensitivity of observers is measured by finding the lowest contrast to see gratings of varied spatial frequencies. Contrast is defined by the difference in luminance or color that makes an object distinguishable. Spatial frequency on the other hand, is a measure of how often sinusoidal components repeat per unit of distance and is expressed in cycles per degree (cpd) of visual angle. In psychophysical experiments, researchers often make use of grating stimuli; gratings with thicker bars represent Low Spatial Frequency (LSF), while thinner bars represent Higher Spatial Frequency (HSF). Generally, HSF gratings must have significantly higher contrast than LSF gratings in order to be adequately processed. At electrophysiological level (EEG), various studies report greater positive amplitudes in the P1 component, and greater negativity in the N1 component in response to HSF compared to LSF stimuli. (Craddock, Martinovic, & Müller, 2013). Moreover, larger latencies between stimulus onset and peak amplitudes in both components were found for HSF stimuli (Awasthi, Sowman, Friedman, & Williams, 2013). Furthermore, various studies found that HSF targets, unlike LSF targets, induce a negative-going peak around 80ms as well, known as the N80 (Boeschoten, Kemner, Kenemans, & van Engeland, 2005). Research indicated that the N80 peak originates from activity in V1 neurons in the visual cortex, and it is relative insensitive to LSF (Ellemberg, Hammarrenger, Lepore, Roy, & Guillemot, 2001). Since the N80 is absent in response to LSF visual targets, and the P1 and N1 peaks are smaller and its latencies shorter, it has been suggested that its analyses require fewer neuronal sources (Craddock et al., 2013).

Prior studies found that vision improves for LSF visual information and impairs at HSF in fear conditions (Bocanegra & Zeelenberg, 2009; Lojowska, Galdwin, & Roelofs, 2015). This is suggested to be evolutionary relevant because, when exposed to fear, humans must quickly categorize coarse visual features in the periphery as threatening or non-threatening. On the other hand, thorough, detailed analyses of fine-grained HSF visual features is disadvantegeous because it is too time-consuming. Neuro-imaging techniques further indicated that the amygdala is quickly targeted in a dorsal, subcortical route that mainly depends on LSF-sensitive magnocellular cells (the M-pathway) in threat-conditions (Cushing, Im, Adams, Ward & Kveraga, 2019).

EEG studies previously reported P1 and N1 modulations in respectively a central occipital cluster (electrodes Oz, O1 and O2) and a lateral parieto-occipital cluster (PO7/PO8) (Pourtois, Sander, Grandjean &

Veuilleumier, 2004) in threat-related trials. The current project at Ghent University further explored these modulations in other, distinct types of fear, resulting in 6 (x2, LSF/HSF = 12) conditions.

Since we only have data from 3 good pilots, we will limit analyses for now on distinct neural responses to LSF and HSF grating stimuli. Reason behind is, there are 12 conditions of each 50 trials per subject. However, should we limit our analyses to LSF/HSF neural responses only, we have 300 trials per condition, per subject. In this way, we have considerably higher statistical power, although still not sufficient for proper statistical analyses for now.

2. Method

2.1. Design and Task

(Right-handed) Participants completed a visual orientation discrimination task. They had to indicate if bars in a grating stimulus (on the screen for 8 frames = 133.33ms) were vertically oriented, or tilted (to the left or right of central fixation). They completed 100 trials per block, 50 LSF (2.0 cpd) and 50 HSF (5.5 cpd) trials in random order. The experimental session comprised 6 blocks, so in total, each participant responded to 600 trials, each lasting 2.7 seconds. In the Bodily Threat blocks (2 blocks), participants were exposed to aversive sounds, in the Psychosocial Threat blocks (2), they were exposed to extreme negative comparative social feedback and no manipulations were implemented in the Control blocks (2). In total, participants responded to 300 LSF trials, and 300 HSF trials. See Figure 1 for a visualization of the trial procedure.

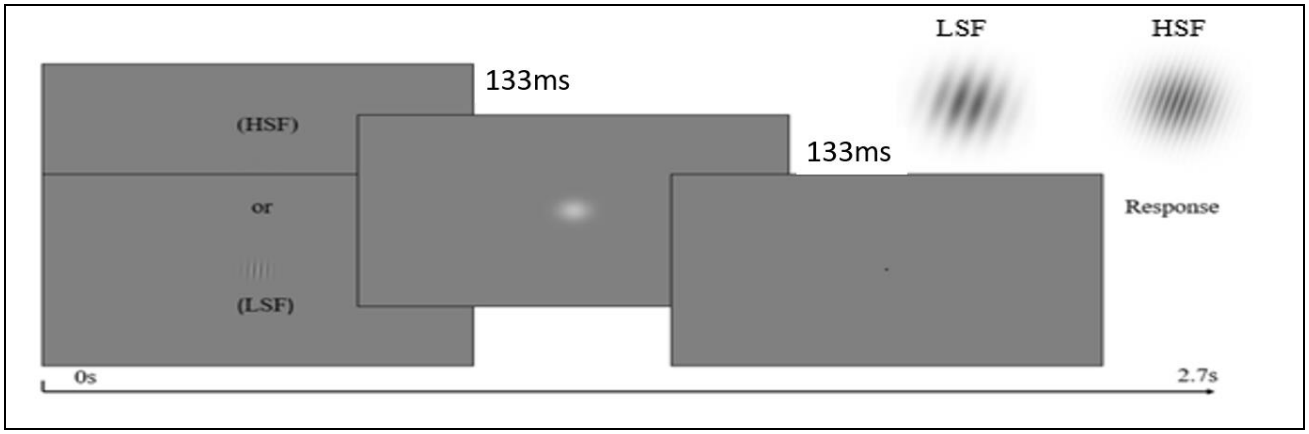

Figure 1. Trial procedure.

2.2. EEG data recording

Continuous EEG was recorded at a sampling rate of 512-Hz using Ag-AgCl (silver-silver chloride) electrodes with a 64-channel ActiveTwo system (BioSemi B. V., Amsterdam, the Netherlands) and were referenced online to the Common Mode Sense (CMS)-Driven Right Leg (DRL) ground. 64 EEG electrodes

were mounted in an elastic cap in accordance to the extended International 10-20 EEG system. 8 Auxiliary electrodes were additionally attached. The horizontal and vertical electrooculography (EOG) signals were monitored by four of these electrodes, positioned above and below the left eye and on each of the outer canthi of the eyes. Two electrodes were placed on the left and right mastoids and the remaining two bipolar electrodes were applied to the volar surfaces of the medial phalanges of the left hand in order to record the Galvanic Skin Conductance Levels (as a measure of fear) throughout the experimental session.

3. Research Questions

The current study aims to identify potential modifications in the N80/P1/N1 ERP-components in threat-related trials compared to neutral trials. Since data is only collected from 3 good pilots yet, we currently limit analyses to LSF and HSF stimuli. We expect to observe a negative-going peak around 80ms in response to HSF trials, but not to LSF trials, in line with previous work. Furthermore, we expect that HSF stimuli evoke larger latencies and stronger peaks in the P1 and N1 component.

4. References

Awasthi, B., Sowman, P.F., Friedman, J., & Williams, M.A. (2013). Distinct spatial scale sensitivities for early categorization of faces and places: neuromagnetic and behavioral findings. *Front. Hum. Neurosci., 7,* 91.

Bocanegra, B.R., & Zeelenberg, R. (2009). Emotion improves and impairs early vision. *Psychol. Sci., 20(6),* 707-713.

Boeschoten M.A., Kemner C., Kenemans J.L., van Engeland H. (2005). Time-varying differences in evoked potentials elicited by high versus low spatial frequencies: a topographical and source analysis. *Clin Neurophysiol, 116,* 1956–1966.

Craddock, M., Martinovic, J., & Müller, M.M. (2013). Task and spatial frequency modulations of object processing: an EEG study. *PLoS One, 8(7),* e70293.

Cushing, C.A., Im, H.Y., Adams, R.B., Ward, N., & Kveraga, K. (2019). Magnocellular and 34 parvocellular pathway contributions to facial threat cue processing. *Soc. Cogn. Affect. Neurosci., 14(2),* 151-162.

Ellemberg D., Hammarrenger B., Lepore F., Roy M.S., & Guillemot J.P. (2001). Contrast dependency of VEPs as a function of spatial frequency: the parvocellular and magnocellular contributions to human VEPs. *Spat Vis., 15,* 99–111.

Lojowska, M., Galdwin, T.E., & Roelofs, K. (2015). Freezing promotes perception of coarse visual features. *J. Exp. Psychol. Gen., 144(6),* 1080-1088.

Pourtois, G., Grandjean, D., Sander, D., & Vuilleumier, P. (2004). Electrophysiological correlates of rapid spatial orienting towards fearful faces. *Cerebral Cortex, 14(6),* 619-633.

Appendix B: The Power Spectral Density (PSD) of All Channels

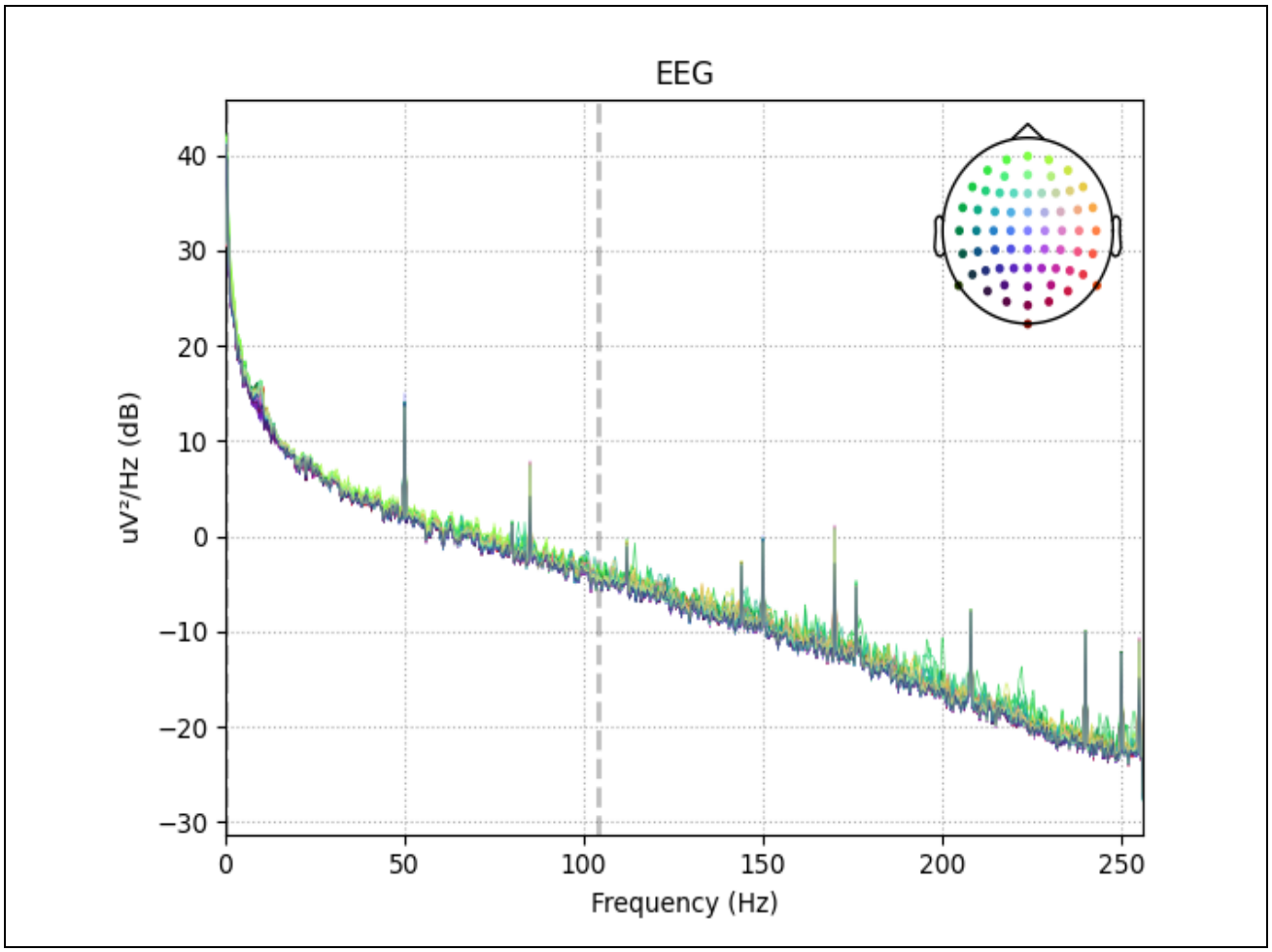

Figure 1. Power Spectral Density (PSD) for all 64 EEG-Channels. No bad channels were identified.

Appendix C: ICA visualizations

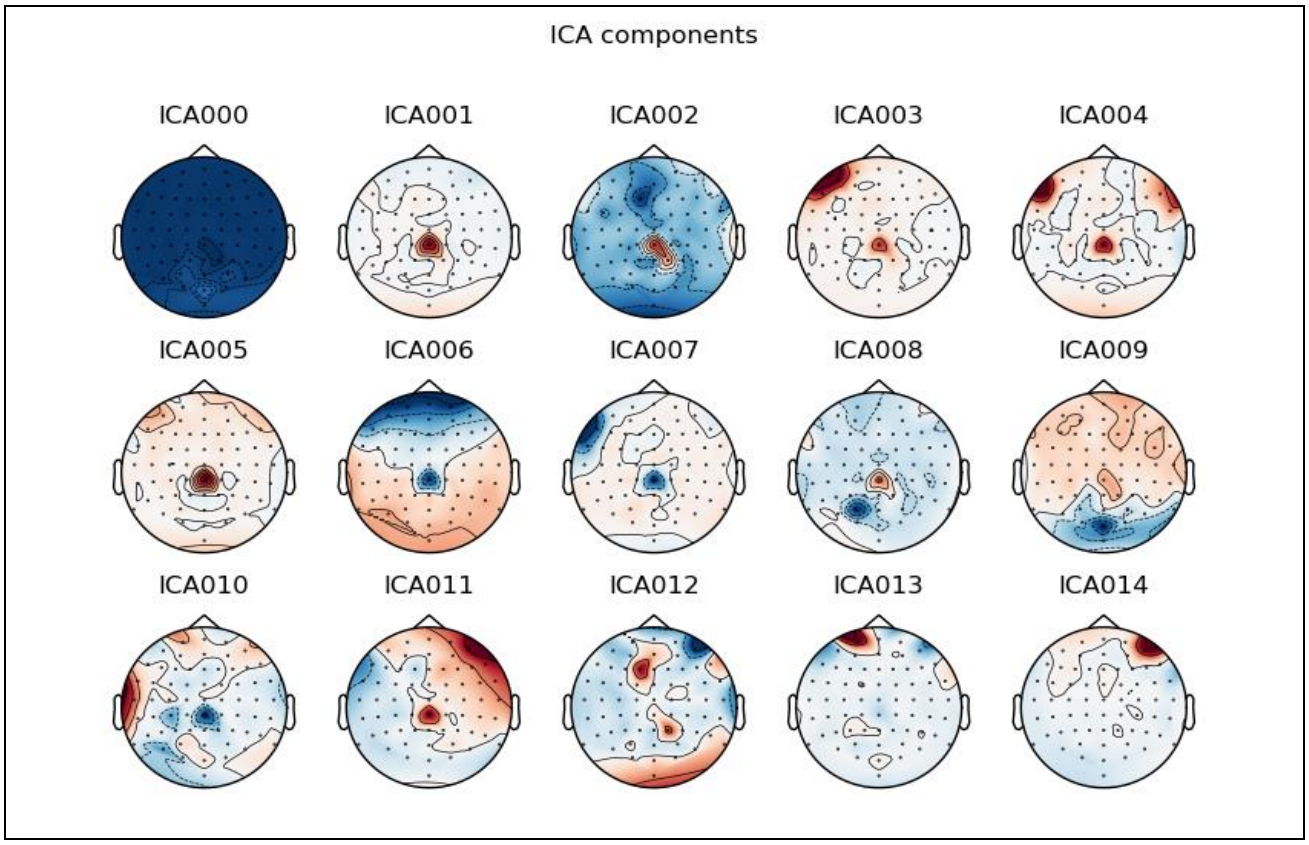

Figure 1. All independent components. We identified component 006 as the component that comprises eyeblinks.

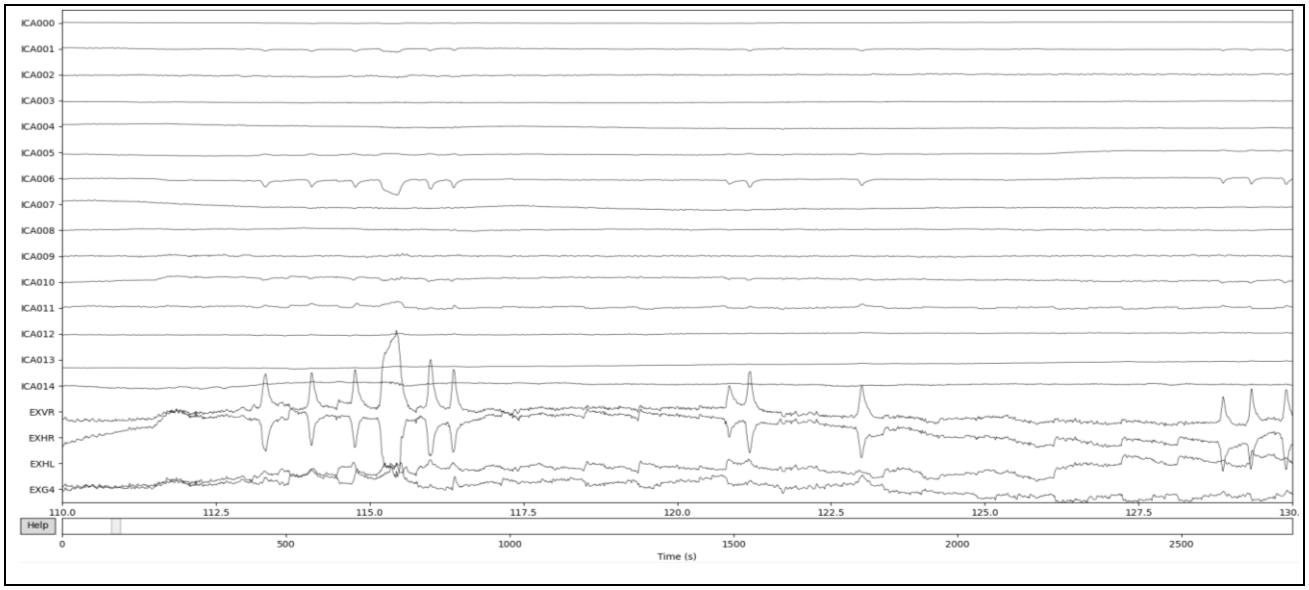

Figure 2. Data segment of all components and EOG channels. Based on this plot, we identified component 006 again as the component that comprises eyeblinks (see the corresponding bursts in EOG channels and in component 006).

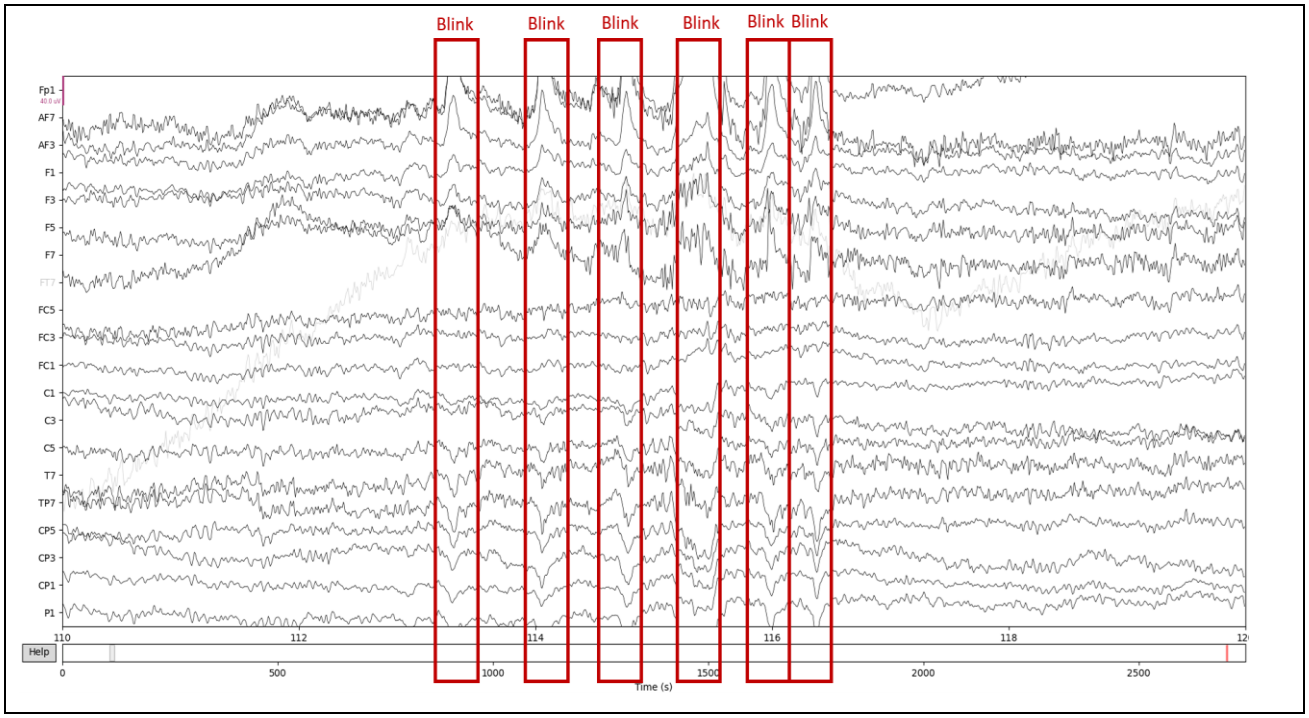

Figure 3. Raw data segment, blinks annotated.

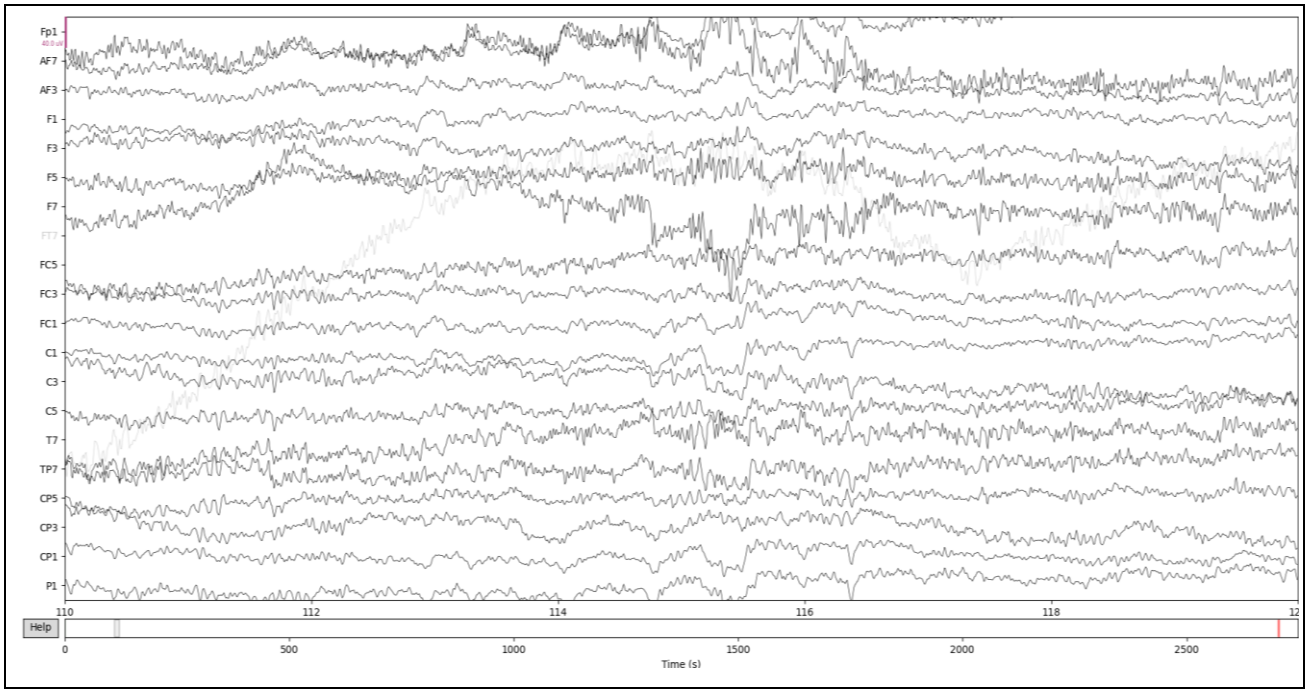

Figure 4. Same data segment as in Figure 3, after ICA was fit on the raw data. Clearly, data is now cleared from eyeblinks.

Appendix D: Grand Average

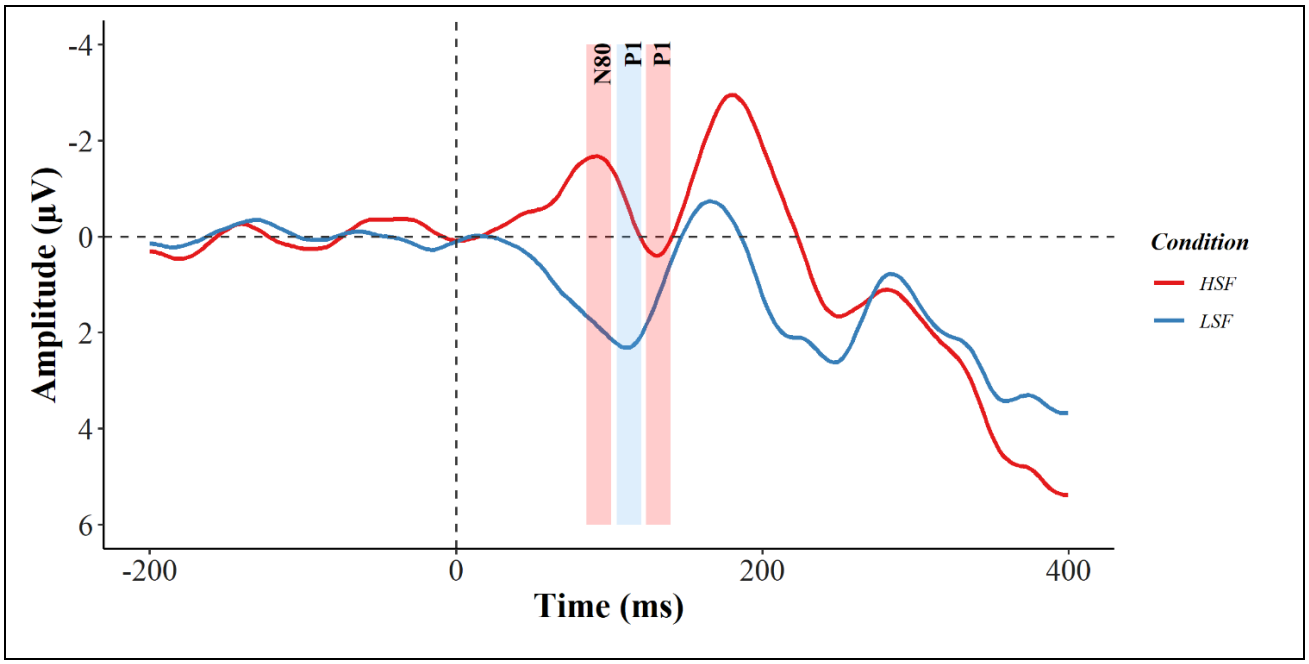

Figure 1. Grand average in the central occipital cluster (electrodes Oz, O1 and O2; strongest P1 and HSF-specific N80 peaks expected). Data was resampled at 20Hz low-pass for visualization purposes. No statistical tests are yet performed.

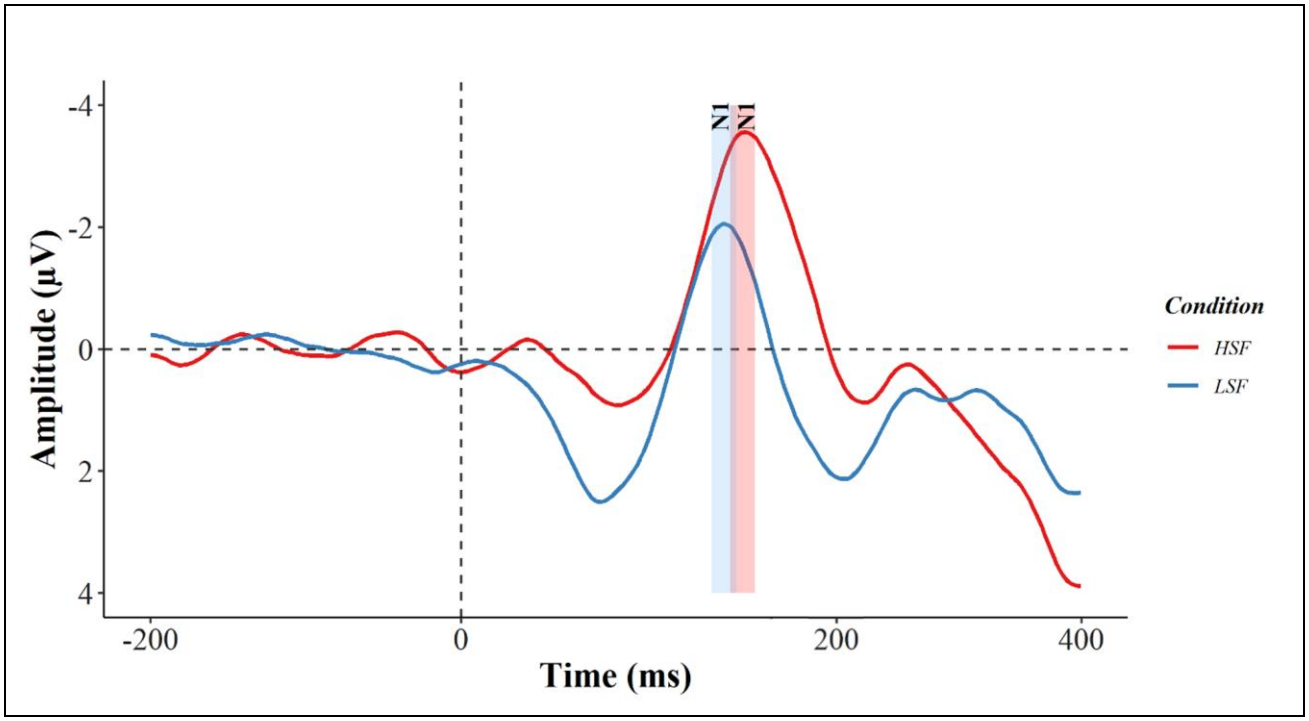

Figure 2. Grand average in the parieto-occipital cluster (electrodes PO7 and PO8; strongest N1 peak expected). Data was resampled at 20Hz low-pass for visualization purposes. No statistical tests are yet performed.

	N80	P100	N100
LSF	64ms 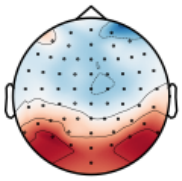	84ms 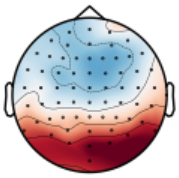	141ms 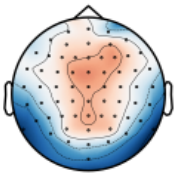
HSF	64ms 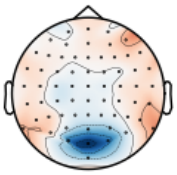	97ms 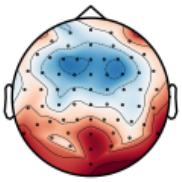	146ms 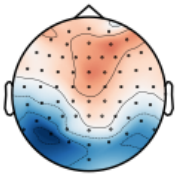

Figure 3. Topographical maps of our 3 ERP components of interest per condition. As for the N80; it seems absent in the LSF condition; amplitudes are already positive-going towards the first (positive) component: the P1 (we included the topographical map for LSF as well to illustrate this point). The latencies of the peaks can be obtained in MNE: condition.get_peak(type='eeg').

Appendix E: Contrast

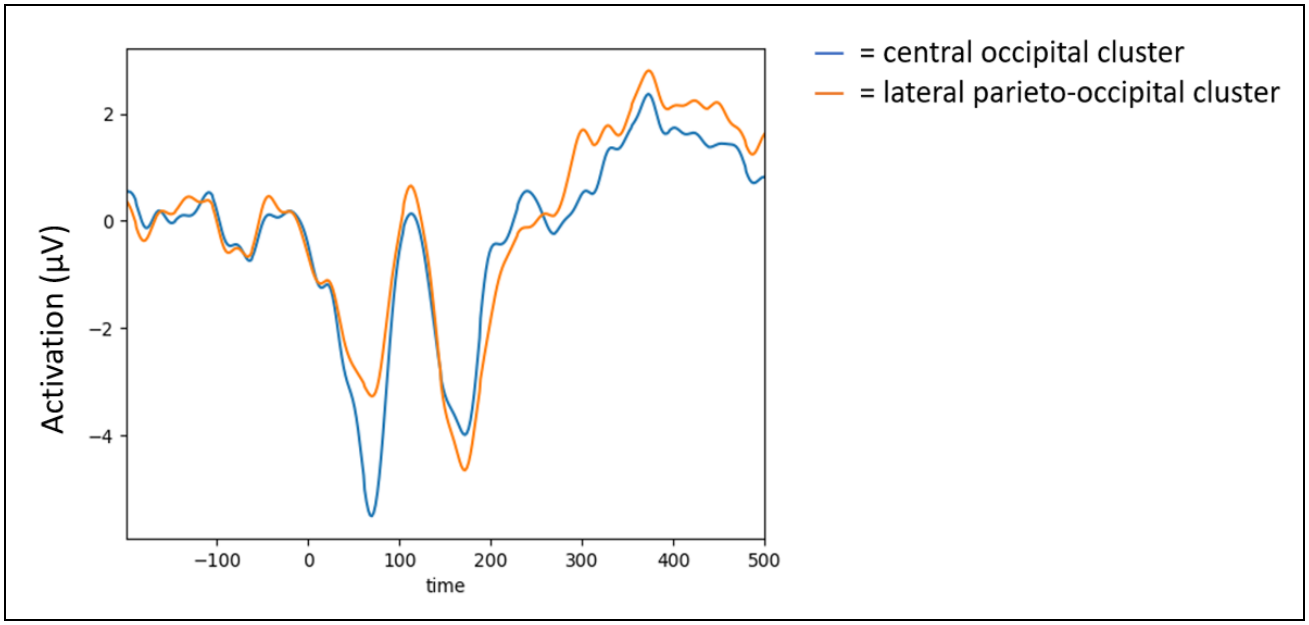

Figure 1. Contrast Activation. No significant clusters were found.

Appendix F: Source Reconstruction Contrast

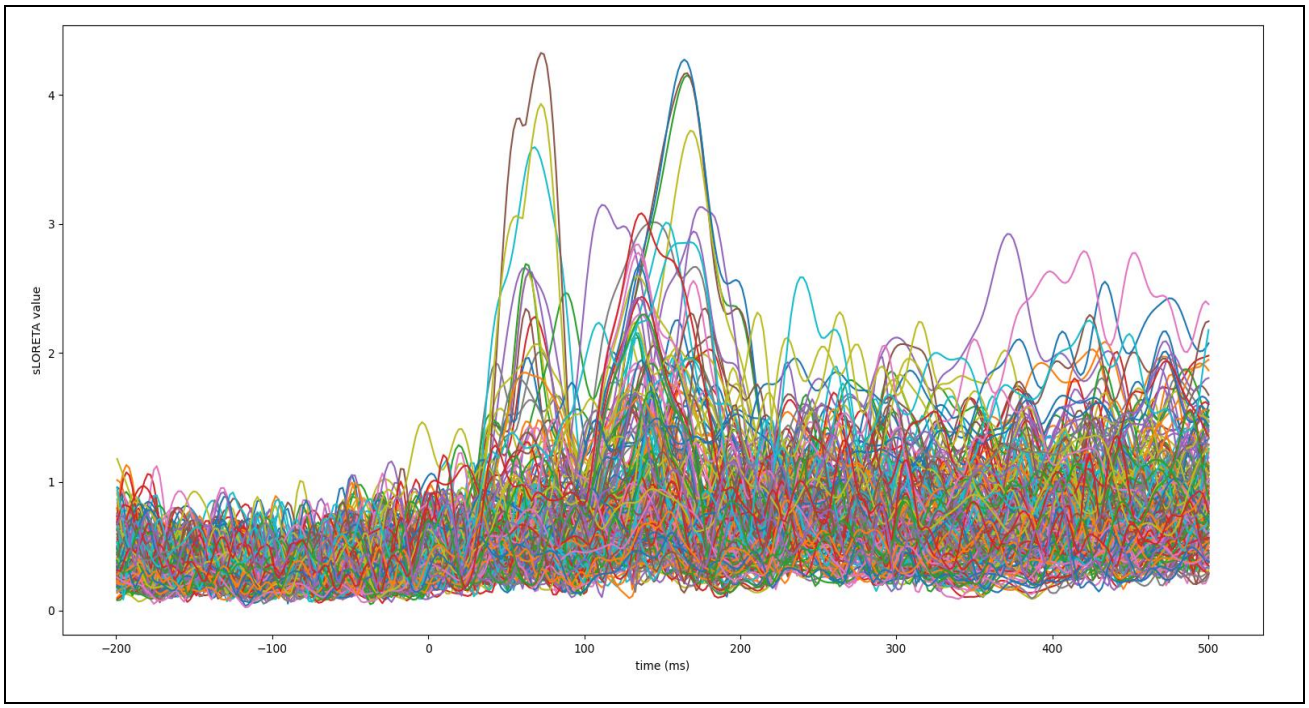

Figure 1. Time series of activation. Y-axis depicts the activation (µV). Colors represent the estimated parameters. Peaks are detected at 72 and 160ms, corresponding to peak activation in the contrast condition (see Appendix E Figure 1. as well).

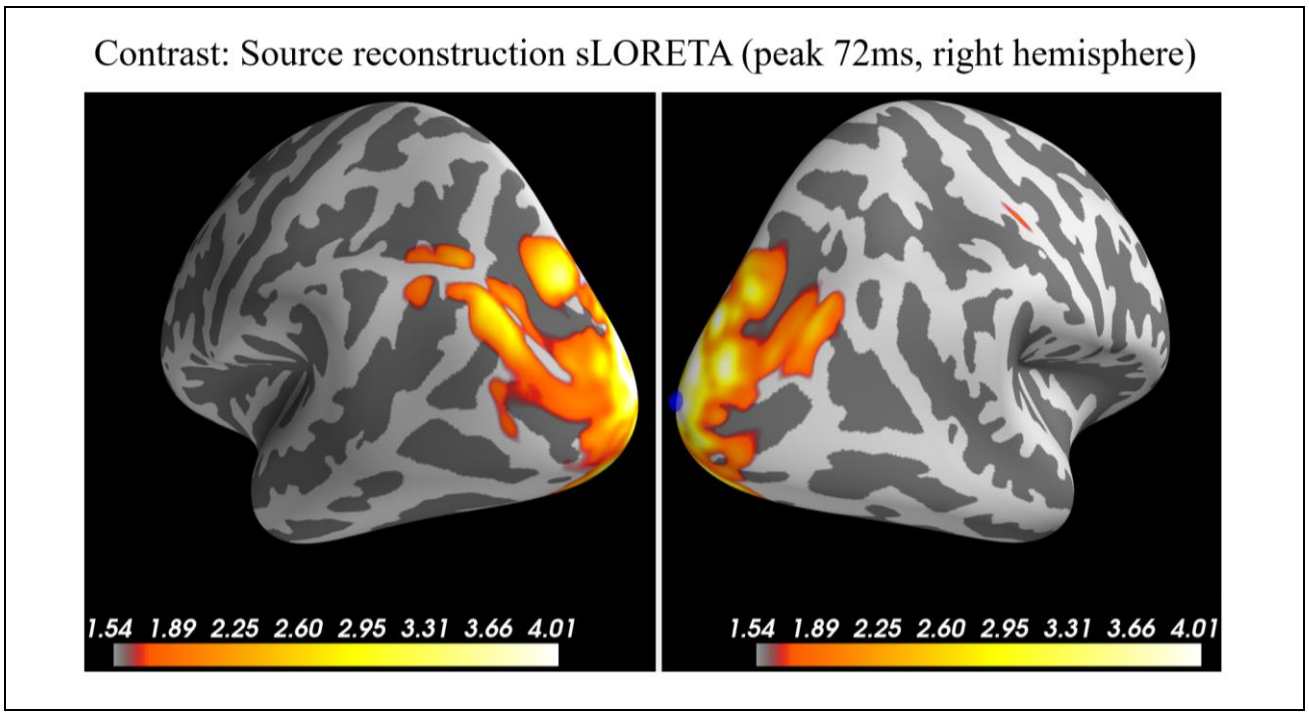

Figure 2. Visualization source reconstruction at peak 72ms. Colors represent activation. Blue dot represents peak of maximal activation (right hemisphere).

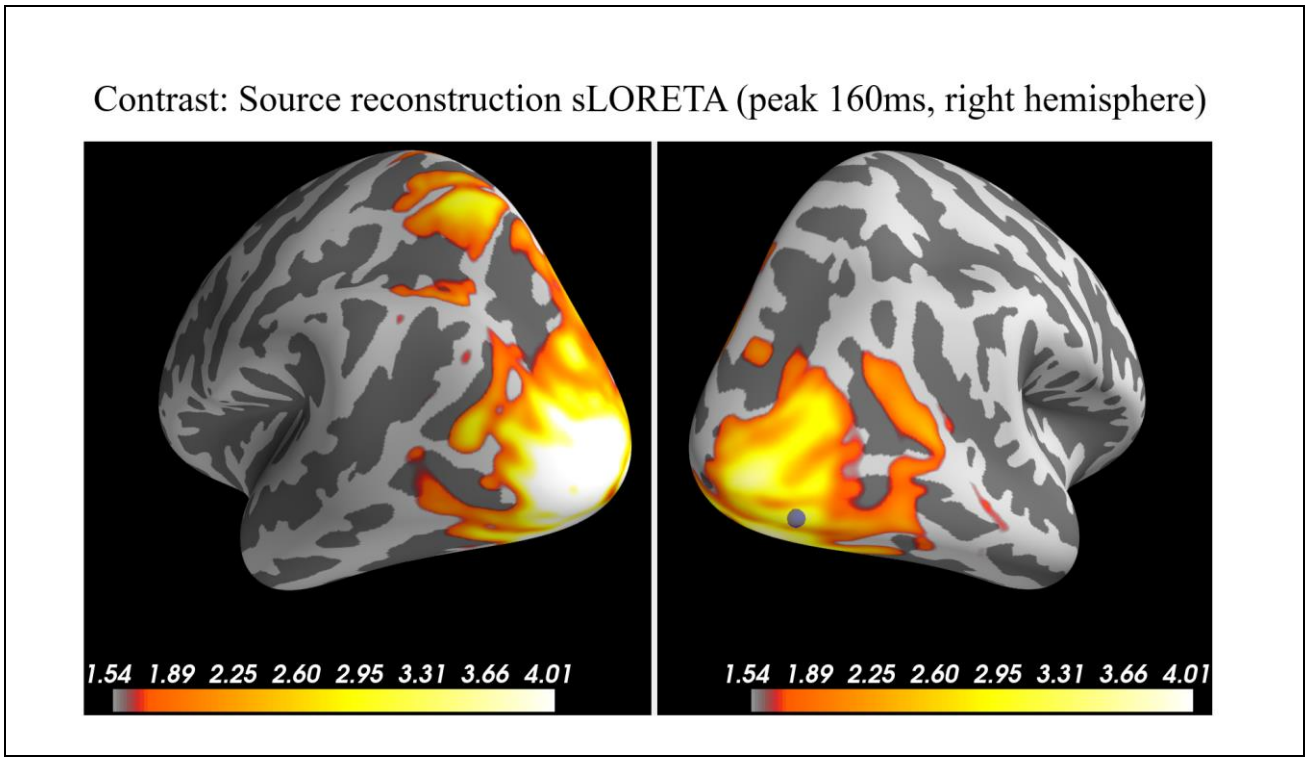

Figure 3. Visualization source reconstruction at peak 160ms. Colors represent activation. Blue dot represents peak of maximal activation (right hemisphere).

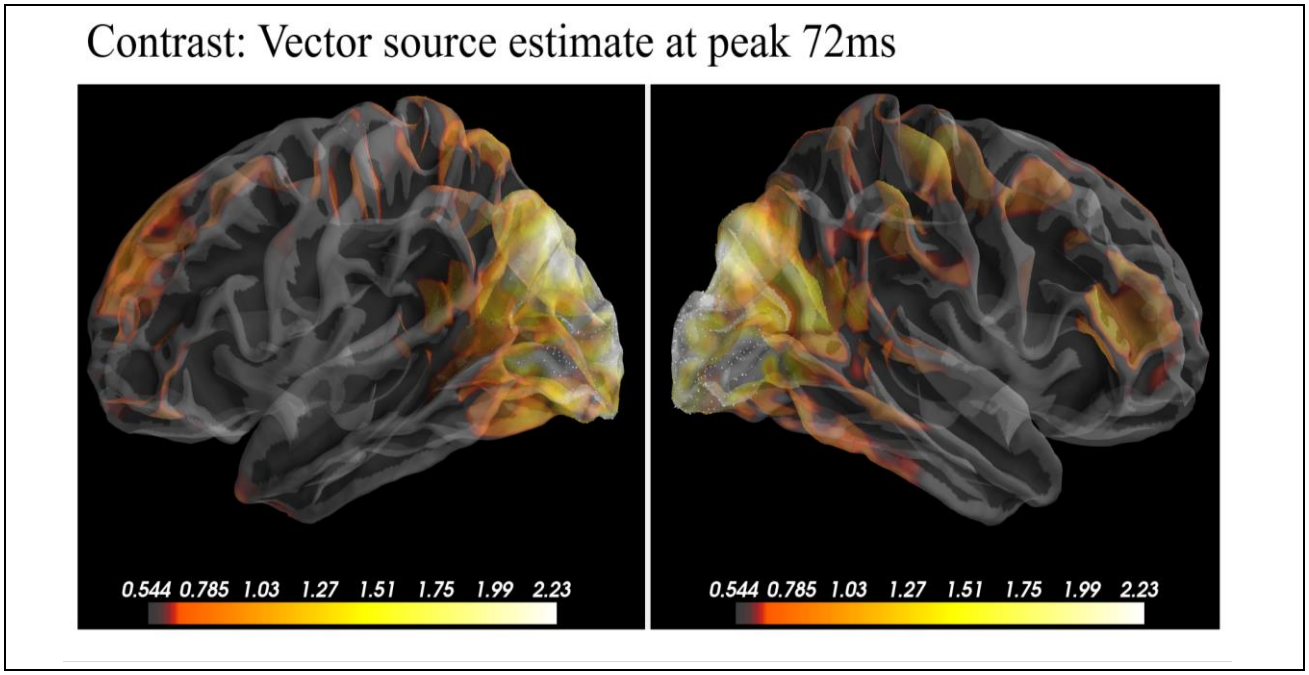

Figure 4. Visualization vector source estimate at peak 72ms.

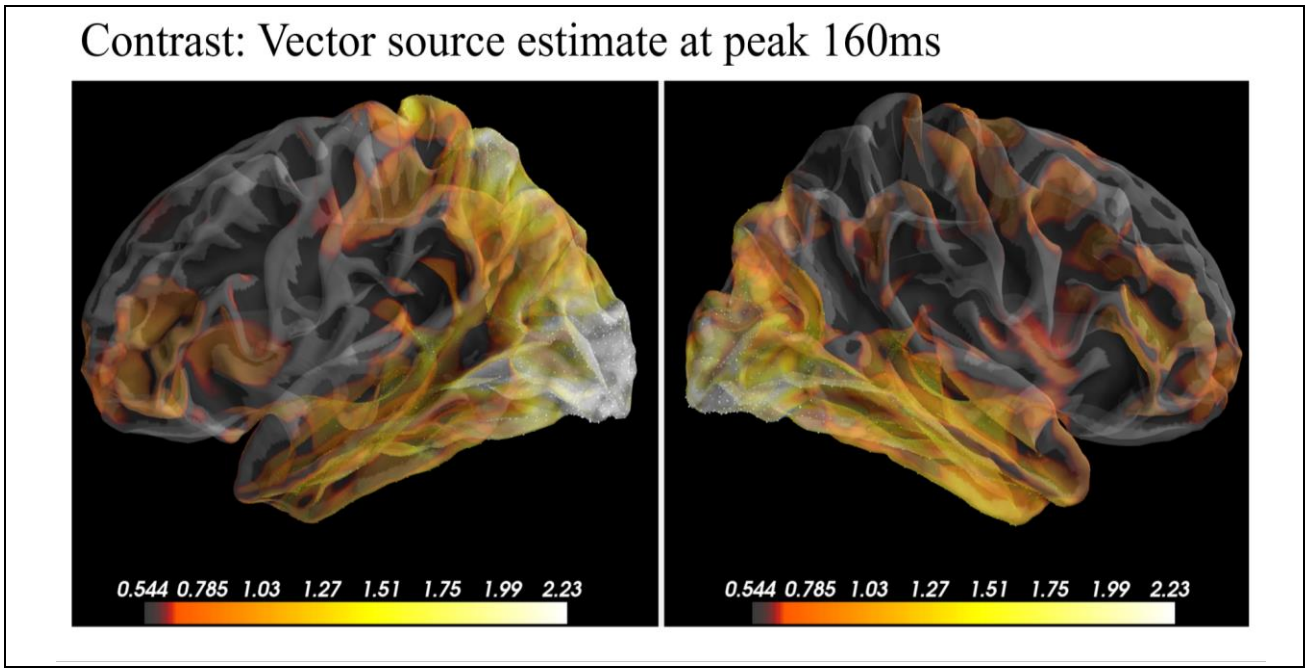

Figure 5. Visualization source estimate at peak 160ms.